Chaotic transients of two particles in a Paul trap: Interpretation as a boundary crisis

J. Hoffnagle and R. G. Brewer
IBM Almaden Research Center, 650 Harry Road, San Jose, California 95120
(Received 8 June 1994)

Calculations based on coupled Mathieu-Coulomb equations indicate that the transition from transient to stationary chaos for two ions in a Paul trap near the edge of the stability region is due to a boundary crisis. Numerical simulations reproduce the long-lived chaotic transients observed in ion trap experiments, obeying the power-law dependence $T(q) \propto (q_c - q)^{-\gamma}$, where T is the average transient lifetime and q the dimensionless trap voltage. The unstable, periodic orbits which are fundamental to a heteroclinic boundary crisis were identified and the intersection of their invariant manifolds in the four-dimensional phase space was located, yielding a prediction for q_c, the transition point between transient and stationary chaos, that agrees well with the experimental value. This provides a theoretical understanding of a transition which previously has been a subject of controversy. Finally, a heuristic derivation is given for the critical exponent γ, based on the stability properties of the mediating periodic orbits. Thus solutions of the deterministic, time-dependent equations of motion can be used to accurately describe the duration of transient two-ion chaos near criticality, with only a single free scale factor.

PACS number(s): 32.80.Pj, 03.20.+i, 52.55.Mg

I. INTRODUCTION

Ever since the first observations of ordered arrays of cold, trapped ions [1, 2], there has been considerable interest in the dynamics of these "ion crystals." Experiments on laser-cooled ions in Paul traps showed that changing the trap parameters could induce abrupt transitions between the crystalline state and a diffuse, extended state of motion [3, 4], which we interpreted as deterministic chaos. While numerical calculations confirmed that the extended "cloud" is indeed chaotic [3–5], the nature of the transitions between order and chaos has remained controversial. The very existence of a control parameter with a critical value was disputed [6] until it was established experimentally [7] that the evolution of the trajectories on long time scales is crucial—the transition observed in Ref. [3] is one between stationary and transient chaos. There is by now an extensive literature of transient chaos, including both experimental and theoretical studies [8]. The observed power-law dependence of the transient lifetime on the control parameter q suggested that the boundary crisis mechanism, explicated in a series of papers by Grebogi and co-workers [9–16], could be responsible for the transition. This paper presents further calculations of the long-time behavior of the two-ion system that agree with the observed chaotic transients. Careful examination of the trajectories at the conclusion of the chaotic transient allows the identification of the unstable, periodic orbits involved in the crisis. Further analysis of the equations of motion locates the manifold intersections postulated by boundary crisis theory, and leads to predictions for the critical parameters of the transition from transient to stationary chaos.

Theoretical investigations of Paul trap dynamics have relied largely on numerical solutions of the equations of motion, though some analytic results are possible in the pseudopotential approximation [17], which replaces the oscillatory trap potential with a static, time-averaged, harmonic well. The integrability of the two-ion pseudopotential model for special values of the parameters [6] has been pursued at some length [18, 19], though details are disputed [20, 21]. Unfortunately, a clear connection between these results and experiments has not been forthcoming, and the justification of secular averaging is questionable for practical conditions under which the "fast" and "slow" frequencies differ by only about a factor of 2. It has also been shown that as long as dissipation is not too large, the dynamics supports a large number of frequency-locked states [22, 23]. Since these solutions have periods that are multiples of the trap potential's, they do not appear in models which replace the time-dependent potential with a time-averaged one. We shall see that similar *unstable* orbits, with periods equal to three times that of the trap potential, are central to the dynamics of the trapped-ion system on long-time scales.

Numerical simulations of the ion motion can accommodate the time dependence of the trapping potential, and also the complexities of laser cooling. They have been applied in several investigations of the order-chaos transition in ion traps [3, 4, 6, 7, 24], including studies of many-ion systems [4, 6, 25, 26]. In Sec. V B we present simulations that reproduce the essential features of the experiments on chaotic transients, at the same time noting that they have important limitations for the study of long-time dynamical evolution, due to the separation of time scales. Despite this drawback, the simulations still provide valuable information about the transition from chaotic to regular motion, by revealing details of the trajectories that are not accessible experimentally. A better understanding of the order-chaos transition relies on the identification and characterization of the un-

stable, periodic orbits responsible for the crisis. This approach addresses the transition at a more elementary level than simulations alone, and also allows more accurate computation of the critical parameters [11, 12, 16]. With the numerical simulations as a guide, we find the crisis-mediating orbits. From their stability properties and the geometry of their invariant manifolds, a theoretical description of the boundary crisis can be derived which agrees well with the experimental data.

The theory of trapped-ion dynamics is further complicated by the role of laser-cooling. The interaction of an ion with a resonant laser beam depends nonlinearly on velocity, leading to a system with two unrelated, nonlinear forces: Coulomb repulsion and radiation pressure. After the latter was used to initiate transitions at low trap voltage in experiments [1, 4], several computational studies have included both the Coulomb and laser-cooling nonlinearities [4,6,24,25]. Laser cooling also has a stochastic component, since photons are absorbed and emitted at random times, and it has been suggested that this could initiate chaos [24], rather than the collisions observed in Ref. [7]. However, the complication of a nonlinear, fluctuating laser-cooling force is not necessary for the existence of order-chaos transitions. One of the first experiments on electrodynamic trapping [27] reported such transitions in ensembles of electrostatically charged particles for which the only damping was linear, aerodynamic drag; since the equations of motion for particles in a Paul trap are scale independent, this observation that the Coulomb nonlinearity alone can give rise to an order-chaos transition applies to trapped ions as well. We therefore consider the observations of Refs. [3] and [7] in the framework of the simple, deterministic system in which the Coulomb force is the sole nonlinearity. The only calculations in this paper that are not purely deterministic are the numerical simulations in Sec. V B, which include a stochastic component as an artifice to destabilize the very shallow frequency-locked attractors. We speculate that the laser-cooling force has a similar effect on trapped ions. The transition from transient to stationary chaos has an entirely different origin, which is to be found in the deterministic, time-dependent equations of motion.

The rest of the paper is organized as follows: Sections II and III review the equations of motion of two ions in a Paul trap and the concept of boundary crises; they also serve to define notation. Section IV analyzes the experimental observations of transient chaos in ion traps and compares them with the predictions of crisis theory. In Sec. V we show the results of numerical simulations, looking first at lifetime scaling and then at the details of the motion in the final moments of the transient. The information thus obtained is used in Sec. VI to describe the boundary crisis in terms of its fundamental, geometrical elements. Section VII summarizes the results.

II. EQUATIONS OF MOTION

A. Mathieu-Coulomb equations for two ions in a Paul trap

The Paul trap [27, 28] is an electrodynamic trap that confines charged particles in an oscillatory, quadrupole potential,

$$V(\mathbf{r}) = (V_{DC} - V_{AC}\cos\Omega t)\,\frac{x^2+y^2-2z^2}{2r_0^2}. \tag{1}$$

The equations of motion for a single particle of charge e and mass m can be expressed in dimensionless form by introducing a new time variable,

$$\tau = \Omega t/2, \tag{2}$$

and dimensionless static and oscillatory potentials,

$$a = \frac{-8eV_{DC}}{mr_0^2\Omega^2}, \tag{3a}$$

$$q = \frac{4eV_{AC}}{mr_0^2\Omega^2}. \tag{3b}$$

With these definitions, the equations of motion of a single particle separate into independent Mathieu equations for the three Cartesian components, $\mathbf{r}(\tau)$,

$$\ddot{r}_i + (a_i - 2q_i\cos 2\tau)r_i = 0; \quad i = 1,\ 2,\ 3. \tag{4}$$

Here $a_1 = a_2 = -a/2$, $a_3 = a$, $q_1 = q_2 = -q/2$, $q_3 = q$, and dots denote differentiation with respect to τ.

The solutions to Eq. (4) are Mathieu functions [29], which are either oscillatory or exponentially divergent, depending on the parameters a_i and q_i. For $a = 0$ stable single-particle motion is possible in the parameter range $0 < q < q_M$, where q_M is numerically determined to have the value $q_M = 0.908\,046\ldots$. In the stable region of parameter space the Mathieu functions may be expanded in Floquet series of the form $\sum_{k=-\infty}^{\infty} c_{2k}e^{\pm i(\beta+2k)\tau}$, where the Floquet exponents β and the coefficients c_{2k} are transcendental functions of the a's and q's, and are therefore generally different for the axial and radial degrees of freedom. Keeping only the $k = 0$ term in the series yields the pseudopotential approximation of the trap as an anisotropic, harmonic well, with secular frequencies (in dimensional units) $\omega_{r,z} = \frac{1}{2}\beta_{r,z}\Omega$.

The motion of two identical particles, with coordinates $\mathbf{r}^{(1)}$ and $\mathbf{r}^{(2)}$ separates into a center-of-mass part, obeying Eq. (4), and a relative part $\mathbf{r}_{12} = \mathbf{r}^{(1)} - \mathbf{r}^{(2)}$, with components (r,ϕ,z) in cylindrical coordinates. Extensive calculations have shown that the essential features of the dynamics are contained in the restricted system with two spatial dimensions (r,z) that corresponds to the special case where the angular momentum about the z axis vanishes, $L_\phi = 0$. The Coulomb force between the particles, $e^2\mathbf{r}_{12}/r_{12}^3$, takes its simplest form if we adopt a natural unit of length,

$$[\ell] = 2\left(2e^2/m\Omega^2\right)^{1/3}. \tag{5}$$

Introducing a linear damping term proportional to a constant Γ (discussed at greater length below) yields the following equations of motion:

$$\begin{aligned} \ddot{r} + \Gamma\dot{r} + \left[q\cos 2\tau - a/2 - (r^2+z^2)^{-3/2}\right] r = 0, \\ \ddot{z} + \Gamma\dot{z} + \left[a - 2q\cos 2\tau - (r^2+z^2)^{-3/2}\right] z = 0. \end{aligned} \tag{6}$$

This pair of coupled, nonlinear differential equations describing the motion of two ions in a Paul trap will be referred to as the *Mathieu-Coulomb* equations. Henceforth we restrict our attention to the special case $a = 0$, leaving one control parameter, q. One regular solution is of special significance; it is denoted the *crystal* because it is the two-ion analog of the regular arrays seen in multiple-ion systems, and it has a simple explanation in the pseudopotential approximation. For $a = 0$ the Floquet exponents satisfy $\beta_r < \beta_z$ and the total pseudopotential is lowest when the two ions lie in the radial plane, $z = 0$. When the relative coordinate is

$$r_c = \beta_r^{-2/3} \tag{7}$$

the average trapping force just balances the ions' electrostatic repulsion. Exact solutions of Eqs. (6) have a regular solution with $r \approx r_c$ that is stable over the range $0 < q < q_M$. (Recent calculations predicting instability of the crystal apply only to $a \neq 0$ [30, 31].) Because of the periodic trapping field the ions oscillate about r_c ("micromotion") with a period equal to that of the trap.

It is often useful to regard a periodically driven system as a discrete mapping of phase space onto itself, rather than a differential equation with a continuous time variable. Equations (6) are equivalent to a flow,

$$d\mathbf{x}/d\tau = \mathbf{f}(\mathbf{x}, \tau), \tag{8}$$

of the four-dimensional phase-space vector $\mathbf{x}$, with components r, z, $\dot{r}$, and $\dot{z}$. Integration of Eq. (8) yields an evolution operator $\mathbf{U}_{\tau,\tau_0}$ that advances a point in phase space through a finite time interval,

$$\mathbf{x}(\tau_0 + \tau) = \mathbf{U}_{\tau,\tau_0}(\mathbf{x}(\tau_0)). \tag{9}$$

Because of the periodicity of the trapping potential, the parameter τ_0 in the evolution operator always can be replaced by $\tau_0 \bmod \pi$. Choosing some conventional starting time, say, $\tau_0 = 0$, repeated applications of $\mathbf{F} \equiv \mathbf{U}_{\pi,0}$ give a representation of the motion as a series of points, each of which is obtained from its predecessor by a mapping of phase space onto itself:

$$\mathbf{x}_{n+1} = \mathbf{F}(\mathbf{x}_n). \tag{10}$$

In this *stroboscopic mapping* a solution $\mathbf{x}(\tau)$ of Eq. (8) is represented by an infinite series $\{\mathbf{x}_n\}$ of discrete points. The crystal, having period π, is a fixed point of the stroboscopic mapping, $\mathbf{F}(\mathbf{x_C}) = \mathbf{x_C}$, and the solutions with period $P\pi$ correspond to repeating sequences of P distinct points, each of which is a fixed point of $\mathbf{F}^P$. In the following, both the differential equations, Eq. (6), or the stroboscopic mapping, $\mathbf{F}$, will be used to describe the ion motion. We try to avoid confusion by reserving symbols such as $\mathbf{x}_A$ for points in the phase space acted on by $\mathbf{F}$, and denoting the corresponding continuous solution as A. The term "trajectory" applies either to a particular solution $(r(\tau), z(\tau))$ of Eq. (6) or the sequence of points obtained from the same initial conditions by a stroboscopic mapping, depending on the context.

B. Energy dissipation

Observations of individual trapped ions were made possible through the use of laser-cooling to restrict the ions' motion to micrometer-sized regions [32] and ion crystals themselves are stable only when the ions' thermal energy is about 200 times smaller than their electrostatic potential energy [33]. For two ions separated by a few μm, this requires effective ion temperatures on the order of 10 mK. Laser cooling enables such low temperatures, but at the price of adding a fundamental complication to the trapped-ion dynamics.

The simplest treatment of laser-cooling considers a two-level ion with energy separation ω_a and linewidth γ_a, illuminated by a plane wave of frequency ω_l and wave vector $\mathbf{k}$. Then the average force on an ion moving with velocity $\mathbf{v}$ is [34]

$$\langle \mathbf{f} \rangle = \frac{\mathbf{k}\hbar\gamma_a}{2} \frac{p}{1+p}, \tag{11}$$

where

$$p = \frac{2\kappa^2}{(\omega_l - \omega_a - \mathbf{k}\cdot\mathbf{v})^2 + (\gamma_a/2)^2} \tag{12}$$

is the saturation parameter, and κ denotes the Rabi frequency. In the limit of small ion velocities, applicable to a well-cooled crystal, Eq. (11) can be expanded in $\mathbf{v}$ to obtain linear damping, $\langle f \rangle/m = -\alpha\hat{\mathbf{k}}\cdot\mathbf{v}$, but in general it is nonlinear in the ion velocity, leading to a system with two nonlinearities: the interionic Coulomb interaction and the ion-optical interaction. The latter can have nontrivial effects for even a single trapped ion [35, 4]. While the laser-cooling nonlinearity is undoubtedly responsible for some transitions that have been seen in ion traps [6, 36], it is not essential to the understanding of the observations of Refs. [3] and [7]. The laser-cooling nonlinearity also couples the center-of-mass and relative coordinates, thereby doubling the dimension of the two-ion phase space. It thus simplifies the theory considerably to replace the light pressure force with a linear, dissipative term, in order to focus on the dynamics of the Coulomb nonlinearity.

As mentioned in the Introduction, *experiments* [27] *indicate that the order-chaos transition is still present when laser-cooling is replaced by linear damping*, $-\Gamma\mathbf{v}$. In this context, it is important that the energy dissipation due to laser-cooling is very small compared to other terms in the ions' equations of motion. Under the conditions of the Ba^+ experiments reported in Sec. IV the parameter α defined in the last paragraph was approximately 4×10^{-3} in the dimensionless units of Eqs. (2) and (5). Moreover, this represents the maximum energy dissipation that laser-cooling can provide. With the usual choices $2\kappa/\gamma_a \sim 1$ and $2(\omega_l - \omega_a)/\gamma_a \sim 1$ the light pressure force drops off rapidly when $\mathbf{k}\cdot\mathbf{v}$ is larger than the linewidth, as is generally the case for chaotic motion. Hence the damping is very weak, and its exact form does not significantly affect the motion. The value of Γ should not be crucial either, provided it is much less than unity. With

the exception of the simulations of Sec. V B, all computations reported in the next sections were performed with $\Gamma = 1 \times 10^{-3}$, which was the smallest value that gave convergence of trajectories to their attractors within a manageably short time.

III. BOUNDARY CRISES

Even small energy dissipation has the important consequence that phase-space volumes contract with time, thus trajectories ultimately tend to attractors [37]. For $a = 0$ there is always at least one regular attractor, namely, the crystal. Stationary chaos implies the existence as well of a chaotic attractor, which is built around unstable periodic orbits [37, 8]. These orbits generally have a saddle-like character, i.e., they are stable with respect to infinitesimal perturbations along some directions in phase space and unstable with respect to perturbations along other directions. Consequently they have both stable and unstable invariant manifolds, which can be loosely defined as the sets of points in phase space that transform into themselves under the flow, Eq. (8), and tend to the periodic orbit in the limits $\tau \to +\infty$ and $\tau \to -\infty$, respectively. In a *boundary crisis* [9] the unstable manifold of an orbit on the attractor (denoted as orbit A) is tangent, at a critical value q_c of the control parameter q, to the stable manifold of an unstable periodic orbit B, lying on the boundary of the basin of attraction of the chaotic attractor. For this geometry the basin boundary is the stable manifold of B. (The orbits A and B need not be distinct. The crisis is called *heteroclinic* if they are and *homoclinic* if not. In a heteroclinic crisis A and B must have the same period [12].) Since the manifolds change smoothly as q is varied, their tangency represents a borderline case between two geometrically different situations: for $q < q_c$ the manifolds intersect, while for $q > q_c$ they do not. The geometry may be visualized more easily if instead of a continuous flow we consider a discrete mapping, such as a stroboscopic map. Then the periodic orbits A and B correspond to fixed points $\mathbf{x}_A$ and $\mathbf{x}_B$, and for a two-dimensional mapping one has the situation shown schematically in Fig. 1. The fixed points each have stable and unstable manifolds, which are represented by the curves W^S and W^U, respectively, and the diagram is drawn for q slightly less than q_c, in which case $W^U(A)$ and $W^S(B)$ intersect at the points $\mathbf{p}$ and $\mathbf{p}'$. With increasing q the intersections approach each other, disappearing above q_c, as illustrated in Fig. 2. Because B is on the basin boundary, the two half-manifolds, $W^{U+}(B)$ and $W^{U-}(B)$, of its unstable manifold evolve very differently. Trajectories leaving $\mathbf{x}_B$ along $W^{U-}(B)$ lead into the chaotic region of phase space, while those following $W^{U+}(B)$ are in the basin of attraction of the crystal and quickly revert to regular motion.

Chaotic transients arise when q decreases through q_c. Then the small loop between $\mathbf{p}$ and $\mathbf{p}'$, which had been part of the chaotic attractor, protrudes into the basin of attraction of the crystal and is removed from the chaotic attractor. Moreover, the infinite series of preimages of this segment is also removed. Even though these segments are small, any trajectory in the chaotic region of phase space eventually reaches one of these "holes" and then rapidly evolves to the crystal. The result is that what had been an attractor for $q > q_c$ becomes a fractal object called a *repeller* [8], since nearby orbits ultimately diverge from it. Orbits near the repeller may, however, remain in its vicinity for a long time before leaving, and during this time a chaotic transient is observed. It can be shown that the lengths of the individual transients are exponentially distributed [10], i.e., the probability of observing a transient of length τ is

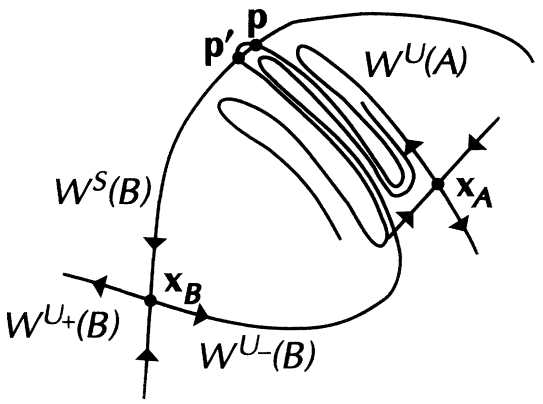

FIG. 1. Schematic representation of a heteroclinic boundary crisis (after Ref. [11]).

$$w(\tau) = \frac{1}{T(q)} \exp[-\tau/T(q)], \tag{13}$$

and that the average lifetime $T(q)$ has a power-law dependence on q [11],

$$T(q) \propto (q_c - q)^{-\gamma}. \tag{14}$$

Aside from a constant of proportionality, the critical exponent γ and the parameter q_c completely describe the divergence of chaotic lifetimes as the control parameter changes. In the next section we shall review the experimental evidence that Eqs. (13) and (14) apply to trapped ions. Subsequent sections discuss the calculation of the critical parameters, first on the basis of simulations and then in terms of the invariant manifolds of the mediating orbits.

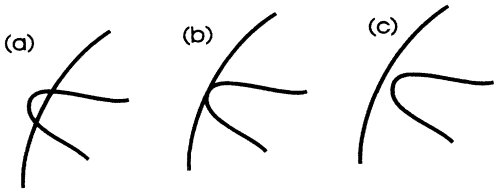

FIG. 2. Detail of the region around the intersection at the top of Fig. 1. The geometry of the manifolds is sketched for (a) $q < q_c$; (b) $q = q_c$; and (c) $q > q_c$.

IV. OBSERVATIONS OF TRANSIENT CHAOS IN AN ION TRAP

Measurements of transient lifetimes were made on barium ions in a Paul trap with $r_0 = 2.5$ mm and $\Omega/2\pi = 3.55$ MHz, and have been briefly described in Ref. [7]. Here we review the experimental data in order to extract quantitative values for the critical parameters that appear in Eq. (14). Ions in the crystalline state were perturbed, either by a collision with a residual gas molecule or by applying a high voltage pulse to the central trap electrode. The ensuing chaotic transient was observed for up to 3 min, i.e., $\tau = 2 \times 10^9$; if the motion was still chaotic after that time, the trap voltage V_{AC} was reduced until the ions recrystallized and the experiment was repeated. Comparison of all the data sets shows no statistically significant dependence of the observed transient lifetimes on the mechanism by which the crystal was perturbed. It is therefore proper to group together all the data taken at a given trap voltage, regardless of how the chaotic transient was initiated.

Figure 3 is a histogram of all transient lifetimes for $q = 0.854$; it is seen to be consistent with an exponential distribution. In principle, a correction for the finite observation time could be made, but it is very small when the average lifetime is much less than the observation time, as in the data of Fig. 3, so we prefer to use the directly measured lifetime. The exponential lifetime distribution was also verified for other values of q. No transients with lifetimes less than 3 min were observed for $q > 0.88$. A few transients were observed for $q = 0.87$ and 0.88 but under these conditions the duration of chaotic motion often exceeded the observation time, so that the data do not yield reliable estimates for $T(q)$. A series of Monte Carlo simulations was performed to address the question of how a power-law distribution, Eq. (14), is distorted by finite observation time. The result was that if the data is limited to points with $T(q)$ less than about one-third of the observation time, the underlying power

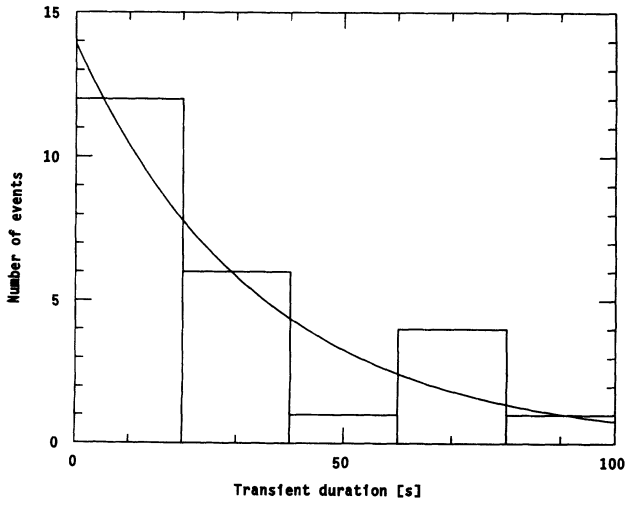

FIG. 3. Distribution of 24 measured transient lifetimes for $q = 0.854$. The curve describes exponential decay with a mean lifetime of 34.5 s.

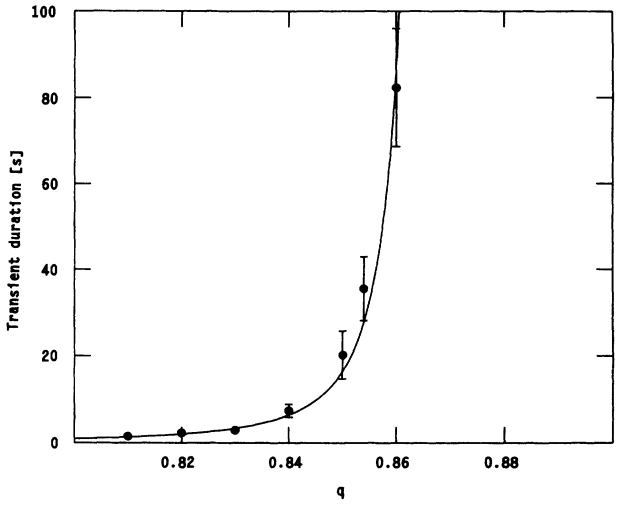

FIG. 4. Measured average transient lifetime as a function of q for two trapped barium ions. The error bars are statistical only. The curve shows the fitted power-law dependence, $q_c^{(expt)} = 0.87$ and $\gamma^{(expt)} = 2.3$.

law can be accurately reconstructed by fitting the measured data without any corrections, whereas larger values of T are badly distorted. The data set of Ref. [7] was therefore restricted to $q \leq 0.86$, for which the measurements showed a monotonically increasing transient lifetime, as illustrated in Fig. 4. These points are in good agreement with a power-law dependence, and a χ^2 fit yields the parameters

$$q_c^{(expt)} = 0.87(1), \tag{15a}$$

$$\gamma^{(expt)} = 2.3(6). \tag{15b}$$

The fit has $\chi^2 = 6.1$ for four degrees of freedom (confidence level 0.19), and is shown in Figs. 4 and 5. The fitted value of q_c agrees with the observed lack of condensation for $q > 0.88$. Although Eq. (14) implies $T(q) \to \infty$

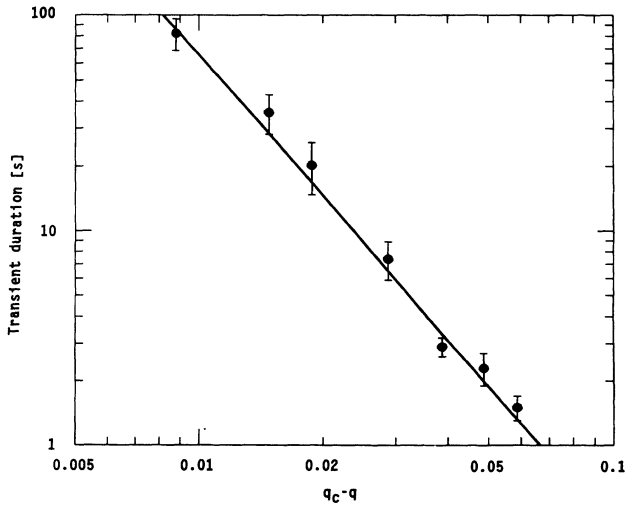

FIG. 5. Measured average transient lifetime vs $(q_c - q)$, with q_c from Eq. (15a).

as q approaches q_c, the presence of noise in physical situations leads to a finite transient lifetime at $q = q_c$ [15]. Referring to Figs. 1 and 2, one sees that noise tends to smooth out the sharp transition in going from $q < q_c$ to $q > q_c$, because fluctuations can transport a trajectory across the basin boundary $W^S(B)$, even in the absence of an intersection with $W^U(A)$. The divergence of $T(q)$ with q led us to propose that a boundary crisis could be responsible for the order-chaos transition in this system [7]. The next sections present evidence to support this interpretation, based first on numerical simulations and then on the geometry of the underlying structures in phase space.

V. NUMERICAL SIMULATIONS

A. Attractors of the Mathieu-Coulomb equations

Straightforward numerical integration of the Mathieu-Coulomb equations commonly yields long, chaotic transients. For instance, $z(\tau)$ for one solution of Eqs. (6) is shown in Fig. 6. When $\tau \lesssim 112\,400\pi$ the particles oscillate erratically in amplitude and phase, the largest Lyapunov exponent is positive, and the Fourier spectrum is continuous [3–6]. Then the irregular motion abruptly gives way to a damped oscillation ending in the crystalline state. A plot of $r(\tau)$ is similar, but also shows a characteristic symmetry breaking upon crystallization: during the chaotic transient r is equally likely to be positive or negative, but after $\tau = 112\,402\pi$ it stays negative forever. Such chaotic transients agree qualitatively with the experimental observations. However, the numerical simulations often terminate on regular solutions which have *not* been seen in ion traps. Before proceeding to a detailed consideration of the computed transients, we must first understand the multiple attractors of Eqs. (6).

The Mathieu-Coulomb equations are remarkable for their plethora of frequency-locked solutions: stable, periodic orbits which close after $\tau = P\pi$, where P is an integer. Each has an attractor with a nonvanishing basin of attraction. Although an example was first given in Ref. [3], the nonobservation of frequency-locking in trapped-ion experiments led to the phenomenon being neglected. Further calculations have shown that frequency-locked attractors are very common in this system; in fact, in the limit $\Gamma \to 0$ their number tends toward infinity as Γ^{-1} [23]. However, except for the crystal (the case $P = 1$), which is stable for $0 < q < q_M$, the frequency-locked orbits are stable over only a limited range in Γ and q, which generally becomes narrower the larger the value of P. Recently, the predicted frequency-locked orbits have been observed in a Paul trap for microspheres, in which aerodynamic drag gives linear damping, as in Eqs. (6) [22].

Though interesting in their own right, the frequency-locked orbits pose a problem for the simulations, since in the trapped-ion experiments the chaotic transients condensed only to the crystal and not to any other attractor. The resolution of this discrepancy [22] is that the frequency-locked attractors are easily destroyed by small perturbations to Eqs. (6). *In this respect only* the nonlinearity due to laser-cooling may play an important role in the evolution of chaotic transients, by preventing the ions from settling into a frequency-locked state. Other perturbations can have the same effect, e.g., higher-order multipoles in Eq. (1), noise on the trapping voltage, or noise added to the ions' positions or velocities. Even linear dissipation destroys the frequency-locked attractors [23]; only the crystal is stable for arbitrarily large Γ.

The behavior of the solutions of Eqs. (6) on long-time

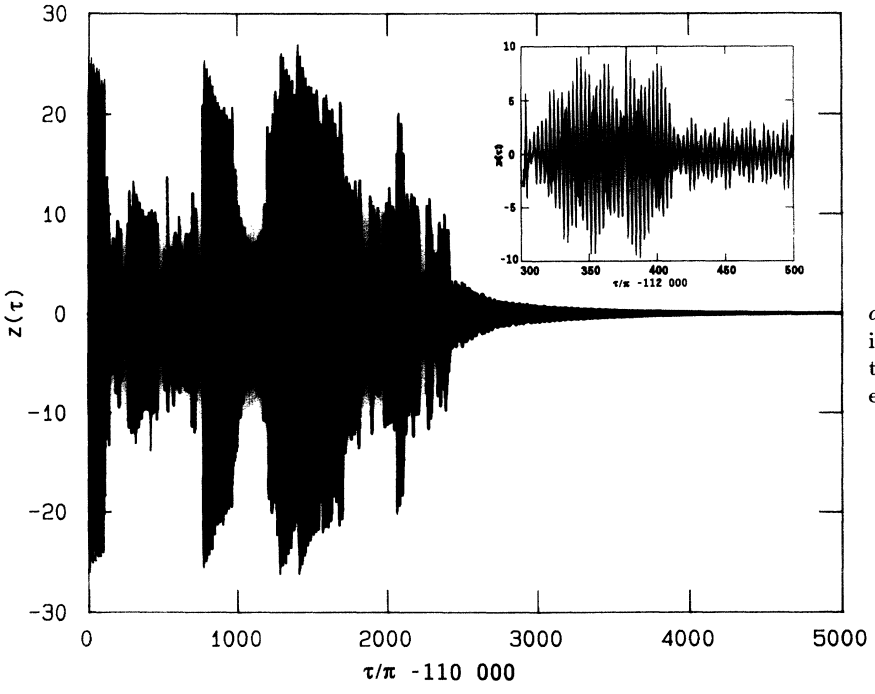

FIG. 6. Numerical solution of Eqs. (6) for $a = 0$, $q = 0.81$, and $\Gamma = 1 \times 10^{-3}$, showing the end of a chaotic transient with a lifetime of approximately $112\,400\pi$. The inset expands the last cycles of the transient.

scales thus agrees with the two-ion experiments, provided that some small perturbation, either deterministic or stochastic, destabilizes the frequency-locked states, leaving the crystal as the only regular attractor. As in the experiments, the chaotic motion is very long lived when q is greater than about 0.88, and otherwise it is transient and ends in crystallization.

B. Lifetime scaling of simulated chaotic transients

Having seen that numerical simulations can model the chaotic transients, we wish to calculate the average lifetime as a function of q. Computations of the average transient lifetime, however, are plagued by the separation of time scales, which also poses difficulties for simulations in celestial mechanics [38] and accelerator dynamics [39]. The trapping potential, Eq. (1), imposes a natural time scale of order unity in dimensionless units, and it is necessary to take a much smaller time step to accurately integrate the equations of motion. However, crystallization takes place on an enormously larger time scale—the data of Fig. 4 extend to $\tau \sim 10^9$. Consequently, the trajectory calculation for even a single chaotic transient requires considerable computation, and extracting the critical parameters by simulating data sets and fitting the q dependence of the transient lifetime to Eq. (14) is a difficult task [14–16]. Nevertheless, numerical simulations are capable of at least qualitatively reproducing the experimental results. To minimize the time-scale problem, the simulations of lifetime scaling used $\Gamma = 3\times10^{-3}$, which is considerably larger than the average rate of laser-cooling for ions in the chaotic state. This leads to faster crystallization, but could also slightly affect the critical parameters.

A series of simulated transients was generated by starting with a set of 50 random initial conditions for the positions and velocities of two ions and numerically solving the Mathieu-Coulomb equations, augmented by a small noise term applied to q, as discussed in Sec. V A. The integration was carried out until the ions either condensed or a predetermined maximum integration time of 1.5×10^7 was reached. The limit on integration time is analogous to the finite observation time in the experiments, but smaller, reflecting limited computational power. After a set of transients was calculated, q was increased in steps of 0.05 until the simulations consistently failed to condense within the allocated time. As in the experiments, the lifetimes obtained for this value of Γ were distributed exponentially, Eq. (13). Condensation was observed for q up to 0.88. Figure 7 shows the results of the simulations, along with a χ^2 fit to a power law, Eq. (14). The best-fit parameters were

$$q_c^{(sim)} = 0.89(1), \tag{16a}$$

$$\gamma^{(sim)} = 1.3(7), \tag{16b}$$

and the fit had $\chi^2 = 5.6$ for six degrees of freedom (confidence level 0.47). The critical exponent is consistent, within the large uncertainty, with the exponent derived from the trapped-ion observations, Eq. (15b). The value of q_c in Eq. (16a) is slightly larger than the experimental value, Eq. (15a), but this may be due to the large damping required to produce crystallization on a time scale accessible to the simulations.

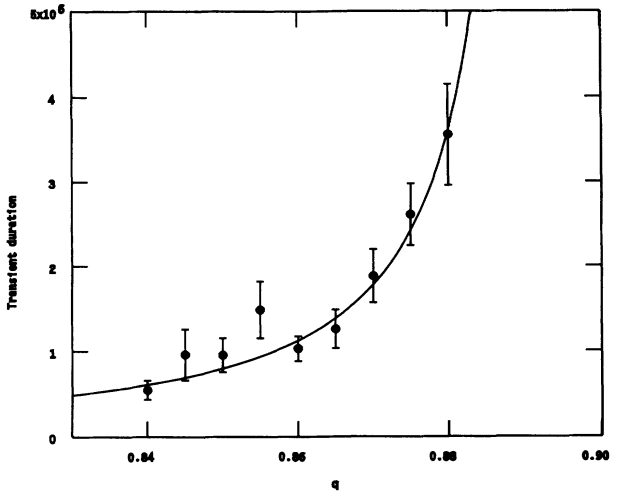

FIG. 7. Transient lifetime (in dimensionless units) as a function of q for the simulations with $\Gamma = 3 \times 10^{-3}$. The curve is the fitted power law, $q_c^{(sim)} = 0.89$ and $\gamma^{(sim)} = 1.3$.

While the results of these simulations are encouraging, the computational effort involved was very great, and even larger sets of simulated lifetimes would be needed to improve the fitted values of the critical parameters. One would also like to know how the critical parameters depend on Γ. Generating even more samples of simulated lifetimes appears impractical; instead more insight into the order-chaos transition can be gained by taking a closer look at the simulated trajectories in the last few trap cycles before crystallization.

C. Terminal phase of simulated chaotic transients

Both experiments and simulations show chaotic transients which scale with q in a manner *consistent* with the boundary crisis scenario. The existence of a boundary crisis, however, implies much more than lifetime scaling, Eq. (14). It gives a detailed picture of how orbits initially near the chaotic repeller find their way into the basin of attraction of the crystal, postulating an intersection of invariant manifolds of one (for a homoclinic crisis) or two (in the heteroclinic case) unstable, periodic orbits. We next consider the question of how this underlying structure of phase space manifests itself in the detailed behavior of chaotic transients.

Although there is no general procedure for identifying the mediating orbits, in some cases they have been found by careful examination of the transient trajectories. The basic idea [12] for a two-dimensional mapping is illustrated in Fig. 8. The invariant manifolds of the unstable fixed points $\mathbf{x}_A$ and $\mathbf{x}_B$ are shown schematically, along with a series of points **a** – **f** on a trajectory at the end

of a chaotic transient. From the discussion of Sec. III we know that the trajectory passes through a region, labeled **pp'** in Fig. 1, where the chaotic repeller pokes into the basin of attraction of the crystal. A point in this region is represented by **d** in Fig. 8. If q is close to q_c, then the area of **pp'** is small, which means that **d** is close to both the unstable manifold of $\mathbf{x}_A$ and the stable manifold of $\mathbf{x}_B$. Since **d** is close to $W^S(B)$, its iterates under the mapping (**e** and **f**) approach the fixed point $\mathbf{x}_B$ before following the branch of $W^U(B)$ that leads to the crystal. Similarly, since **d** is close to $W^U(A)$, some of its preiterates are in the vicinity of $\mathbf{x}_A$. Consequently, there are some points on the trajectory (**b** and **c**) which lie in the neighborhood of $\mathbf{x}_A$, while others (**e** and **f**) are close to $\mathbf{x}_B$. Expressed in the language of continuous flows, rather than discrete mappings, Fig. 8 suggests that the trajectory may briefly approximate the unstable periodic orbits A and B before condensing to the crystal. Short segments of the trajectory provide a glimpse of the underlying periodic orbits, despite their instability. While there is no guarantee that the mediating orbits will emerge from inspection of the chaotic transients, instances in which this fortunate situation obtains have been demonstrated both numerically [12] and experimentally [13, 14].

This approach was applied to long chaotic transients, obtained by numerical integration of Eqs. (6) without any stochastic component. Recall that the end of the transient is marked by symmetry breaking: after some time, e.g., $\tau = 112,402\pi$ in Fig. 6, the radial component of the relative ion position remains either positive or negative forever. Stroboscopic mappings of the transients near this value of τ showed approximate recurrences after three trap cycles. Threefold sequences appeared in many transients, at several values of q, and when the coordinates of such triplets were used to initialize a Newton's method search for periodic orbits [40], the algorithm converged to either of two unstable, period-3π orbits, which

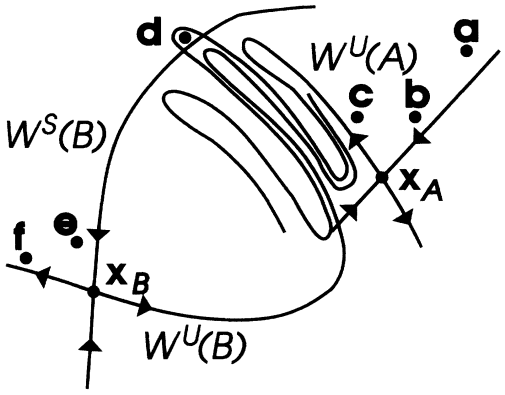

FIG. 8. Schematic illustration of the geometry of phase space for $q < q_c$, near a heteroclinic boundary crisis. The curved lines represent the invariant manifolds of the fixed points $\mathbf{x}_A$ and $\mathbf{x}_B$ of a stroboscopic mapping; these fixed points correspond to the mediating periodic orbits of the full differential equations. The points **a** – **f** depict a trajectory leading from the neighborhood of the chaotic repeller into the basin of attraction of the crystal.

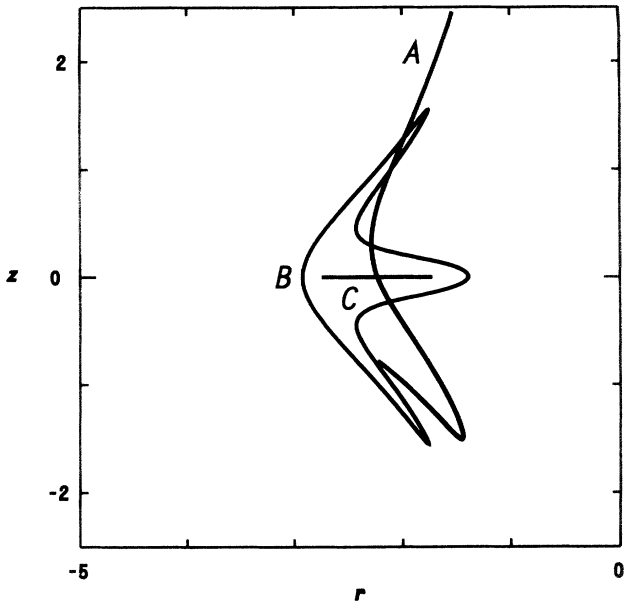

FIG. 9. Trajectories in the r-z plane of the unstable, period-3π orbits A and B for $q = 0.863$. Also shown is the stable, period-π orbit, i.e., the crystal with its micromotion.

are shown in Fig. 9. The simulated trajectories always followed first A then B, as in the schematic representation of a heteroclinic boundary crisis, Fig. 8. The equality of periods for A and B also satisfies an important theoretical requirement [12]. The next section presents additional arguments supporting the identification of the orbits A and B.

A close view of the end of a chaotic transient shows how the mediating orbits "guide" the trajectory from the chaotic repeller into the basin of attraction of the crystal. Figure 10 shows $r(\tau)$ and $z(\tau)$ for a solution of Eqs. (6), each frame representing a segment of the trajectory that covers three cycles of the trapping potential. The frames (a) – (f) of Fig. 10 correspond approximately to the phase-space points **a** – **f** in Fig. 8, if the latter is now regarded as representing the thrice-iterated stroboscopic mapping, $\mathbf{F}^3$. Prior to frame (a) the trajectory oscillates wildly, but in (b) it clearly resembles the unstable orbit A. The approach to A is even closer in frame (c). In frame (d) the trajectory starts close to A, then crosses over to follow the orbit B, and in frames (e) and (f) it has the three-lobed shape characteristic of B. Afterwards, the motion gradually decays to the crystalline attractor, retaining its basic shape while the two lobes extending away from the r axis collapse inward. After a few hundred trap cycles, only the radial micromotion remains.

VI. PREDICTION OF TRANSIENT BEHAVIOR FROM PHASE-SPACE GEOMETRY

The identification of the unstable, periodic orbits that mediate the boundary crisis opens the possibility of relating the observed transient behavior to the geometrical properties of the mediating orbits' invariant manifolds,

without recourse to numerical simulations. If, for instance, it is possible to locate the intersection of $W^U(A)$ and $W^S(B)$, then the critical parameter q_c can be found as the value of q for which the intersection becomes a tangency, rather than by fitting transient lifetimes to a power law [16]. This approach has the important advantage of circumventing the time-scale problem discussed at the beginning of Sec. V B. The reason is that although the duration of chaotic transients diverges near criticality, the manifolds transform smoothly in phase space as q is varied, and the difficulty of locating their intersection remains essentially constant. The critical exponent γ can also be derived from the stability properties of the mediating orbits in the case of a two-dimensional mapping, and the derivation has been extended to some higher-dimensional mappings [12]. Except for an overall scale factor, the parameters q_c and γ completely determine the lifetime divergence as transient chaos becomes stationary. Crisis theory therefore has the potential to provide a complete description of this transition, provided that the invariant manifolds of the mediating orbits can be found.

For two-dimensional mappings, it is possible to construct the invariant manifolds as suggested in Fig. 1 and find their intersections graphically [16]. The analogous picture for our dynamics, however, would represent the intersection of elaborately folded hypersurfaces in a four-dimensional phase space. Without attempting to visualize this complicated geometry, it is possible to gain some important information about the invariant manifolds from the linearized motion in the neighborhood of the periodic orbits. Recall that an orbit of period $P\pi$ corresponds to a fixed point $\mathbf{x}_0$ of the P-fold iterated stroboscopic mapping. The *monodromy matrix* of the periodic orbit, $\mathbf{M}$, defined by

$$\mathbf{M} = \frac{\partial \mathbf{F}^P(\mathbf{x}_0)}{\partial \mathbf{x}_0}, \tag{17}$$

describes the linearized mapping in the neighborhood of

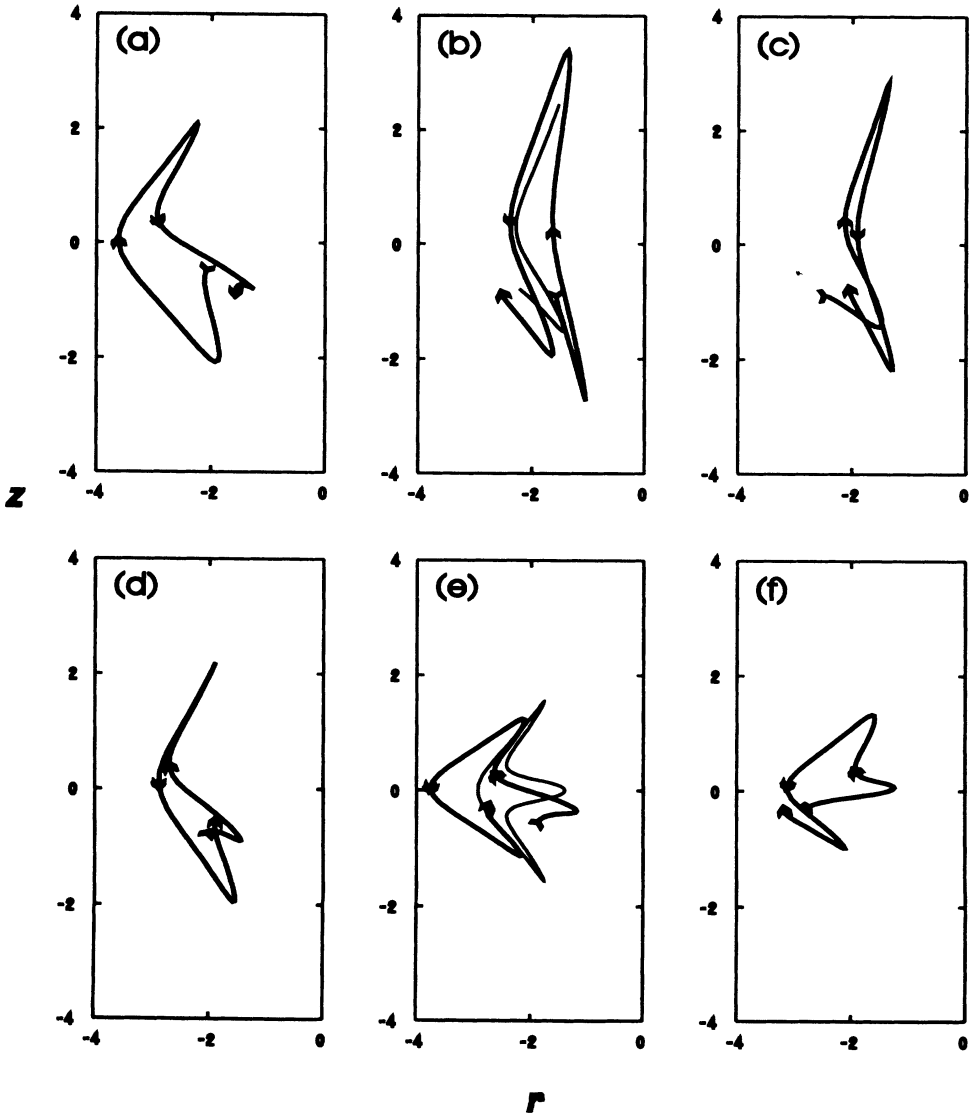

FIG. 10. Sequence of trajectories in the r-z plane at the end of a computed chaotic transient. The parameters were $q = 0.863$ and $\Gamma = 1 \times 10^{-3}$. Each frame follows the trajectory through three periods of the trap potential, with arrowheads indicating the coordinates at $\tau = 0 \bmod \pi$. The thin curves in frames (b) and (e) are the unstable, period-3π orbits A and B from Fig. 9.

$\mathbf{x}_0$. That is, for an infinitesimal perturbation $\delta\mathbf{x}$, $\mathbf{F}^P$ maps the point $\mathbf{x}_0 + \delta\mathbf{x}$ onto $\mathbf{x}_0 + \delta\mathbf{x}'$, with

$$\delta\mathbf{x}' = \mathbf{M} \cdot \delta\mathbf{x}. \tag{18}$$

The monodromy matrix has, for our four-dimensional phase space, four eigenvalues λ_i, which can be denoted as stable or unstable, according to whether $|\lambda_i|$ is less than or greater than 1, respectively. The corresponding eigenvectors $\mathbf{V}_i$ define local, linear manifolds [40] which are tangent at $\mathbf{x}_0$ to the full invariant manifolds of the mapping $\mathbf{F}^P$. Therefore the number of stable (unstable) eigenvalues is equal to the dimension of the stable (unstable) manifold.

The eigenvalues of the monodromy matrices for the mediating orbits identified in the preceding section are listed in Table I. Because $\Gamma \ll 1$ the eigenvalues appear in multiplets resembling those of symplectic matrices, which are organized in one of three ways [39]: (1) complex 4-tuples λ, λ^*, $1/\lambda$, and $1/\lambda^*$ with $|\lambda| \neq 1$ and $\mathrm{Im}\lambda \neq 0$; (2) real pairs λ and $1/\lambda$; and (3) complex pairs λ and λ^* with $|\lambda| = 1$. Consider first the orbit B, the monodromy matrix of which has three eigenvalues of magnitude less than unity, implying that its stable manifold is a three-dimensional hypersurface. This satisfies the theoretical postulate that for $q > q_c$ the basin of the chaotic attractor is bounded by $W^S(B)$, which obviously must have dimension 3 in order to separate the four-dimensional phase space into disjoint regions. As discussed in Sec. III, the one-dimensional, unstable manifold, $W^U(B)$, can be broken into two half-manifolds, which extend from $\mathbf{x}_B$ in the directions $\pm\mathbf{V}_1$. A small displacement from $\mathbf{x}_B$ in these directions places a point either just inside or just outside of the basin of attraction of the crystal. Figure 11 shows how trajectories starting at $\mathbf{x}_B \pm 10^{-3}\mathbf{V}_1$ evolve over the next 30 trap periods. Depending on the sign of the perturbation, the trajectory either gradually approaches the crystal or bursts into chaotic motion, in agreement with the interpretation that B lies on the boundary between the regular and chaotic regions of phase space.

The monodromy matrix of A has two complex pairs of eigenvalues: λ_U, λ_U^* with $|\lambda_U| > 1$; and λ_S, λ_S^* with $|\lambda_S| < 1$, hence the stable and unstable manifolds in this case are both two-dimensional hypersurfaces. The intersection $W^U(\mathbf{x}_A) \cap W^S(\mathbf{x}_B)$, if it exists, must be a one-dimensional loop in phase space. Even though the full manifolds are impossible to visualize, it is possible nevertheless to generate *rays* on $W^U(A)$ and $W^S(B)$ by starting in the neighborhood of the fixed points, where the manifolds are approximately linear, and applying the mapping $\mathbf{F}^3$ or its inverse. If for $q < q_c$ two such rays intersect, the intersection required for a boundary crisis is established. In general, finding the intersection of two hypersurfaces in a four-dimensional space would be a daunting task, but fortunately the simulated transients provide a good indication of where to look; for instance, Sec. V C discussed in some detail the route that one particular trajectory follows from the neighborhood of orbit A to that of B. Taking initial values from Fig. 10, rays on the invariant manifolds were generated, starting near the fixed points on the linear spaces spanned by the appropriate eigenvectors. An empirical criterion for "nearness" is that the linear mapping Eq. (18), be identical to within some small factor ($\sim 1\%$) with the exact mapping $\mathbf{F}^3$. The starting points on the linear spaces were then iteratively adjusted with a function-minimizing routine [41] to reduce the distance of closest approach of the rays, until they intersected to within computational accuracy.

As the parameters of the Mathieu-Coulomb equations are varied, the locations of the fixed points and their manifolds move smoothly in phase space. Therefore a point on the intersection $W^U(\mathbf{x}_A) \cap W^S(\mathbf{x}_B)$ can serve as a starting point for an iterative intersection search with different parameters, provided the parameter change is small. With a fixed value of $\Gamma = 1 \times 10^{-3}$, the parameter q was increased in steps of 2×10^{-4} until the procedure failed to locate an intersection, yielding an estimate of the critical parameter,

TABLE I. Eigenvalues of the monodromy matrix for the mediating orbits A and B at the critical value $q_c = 0.869$. The damping parameter is $\Gamma = 1 \times 10^{-3}$.

Eigenvalue	Orbit A	Orbit B
λ_1	$0.099 - 1.815i$	3.485
λ_2	$0.099 + 1.815i$	$0.077 - 0.992i$
λ_3	$0.030 - 0.544i$	$0.077 + 0.992i$
λ_4	$0.030 + 0.544i$	0.284

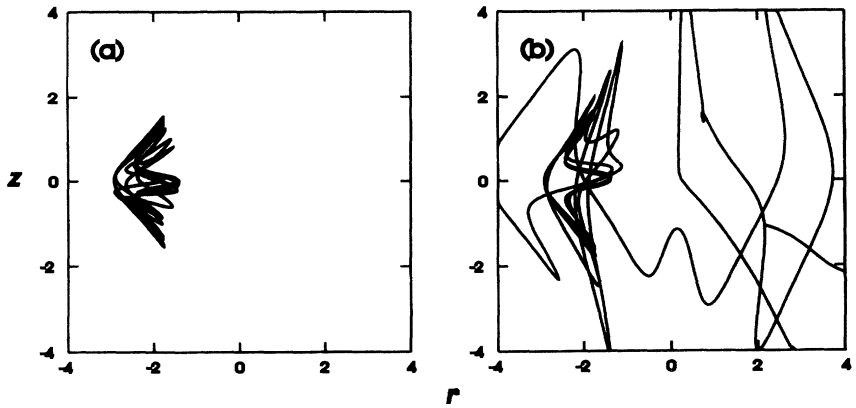

FIG. 11. Evolution of trajectories from the neighborhood of the boundary orbit, B. The initial conditions are (a) $\mathbf{x}_B + 10^{-3}\mathbf{V}_1$ and (b) $\mathbf{x}_B - 10^{-3}\mathbf{V}_1$.

$$q_c^{(th)} = 0.869, \tag{19}$$

that is in excellent agreement with the value of 0.87 ± 0.01 for the trapped-ion experiment, Eq. (15a).

For two-dimensional mappings, it has been shown that the critical exponent γ in Eq. (14) can be expressed in terms of the eigenvalues of the monodromy matrix of $\mathbf{x}_A$ [11]. This result was extended in Ref. [12] to heteroclinic crises in mappings of arbitrary dimension D, for a geometry in which the unstable manifold of $\mathbf{x}_A$ has dimension $D-1$. Unfortunately, this does not apply to our system, for which $D = 4$ and $W^U(A)$ has dimension 2. In the Appendix the argument of Refs. [11, 12] is adapted to the geometry of the present problem with the additional assumption that the points originating near the repeller which escape to the crystal lie in a band of some characteristic width around $W^U(A)$. That assumption leads to the following expression for the critical exponent:

$$\gamma = -2 \ln |\lambda_U| / \ln |\lambda_S|. \tag{20}$$

The frictional damping term that appears in Eqs. (6) implies that phase-space volumes contract uniformly in time; consequently the eigenvalues of the monodromy matrix for a period-$P\pi$ orbit satisfy

$$\sum_{i=1}^{D} \ln |\lambda_i| = -2P\pi\Gamma. \tag{21}$$

Inserting Eq. (21) with $P = 3$ into Eq. (20) yields a theoretical value for the critical parameter,

$$\gamma^{(th)} = 2\,(1 + 3\pi\Gamma / \ln |\lambda_S|)\,. \tag{22}$$

For $\Gamma \ll 1$ the critical exponent is slightly less than 2 (from Table I, $\gamma^{(th)} = 1.99$) in agreement with the unconstrained fit to the lifetime scaling data, Eq. (15b). If the parameters in Eq. (14) are constrained to the values of Eqs. (19) and (22), then the experimental transient lifetimes can be fitted with only one free parameter (a proportionality constant). In this case the confidence level of the fit rises to 0.30 ($\chi^2 = 7.25$ for six degrees of freedom), indicating good agreement between experiment and the boundary crisis prediction.

VII. CONCLUSIONS

Exact solutions to the Mathieu-Coulomb equations support the interpretation of Ref. [7] that the order-chaos transition at $q = 0.87$ observed in ion trap experiments is due to a boundary crisis. Guided by numerical simulations, the unstable periodic orbit B lying on the boundary of the regular attractor was located, as was the nearby orbit A on the chaotic repeller. The two mediating orbits have the same period, as required for a heteroclinic boundary crisis. One question that remains for further investigation is why these particular orbits, out of the infinite number of unstable periodic orbits, should play the central role in the crisis. Points of intersection of the invariant manifolds $W^U(A)$ and $W^S(B)$ were located, fulfilling a central postulate of boundary crisis theory, and permitting the critical parameter q_c to be predicted. Finally a heuristic derivation of the critical exponent in terms of the stability properties of the mediating orbit A completes an accurate description of the experimentally observed lifetime scaling, based on the geometrical properties of fundamental phase-space structures. We emphasize that these results are grounded entirely on the deterministic Mathieu-Coulomb equations, without any stochastic terms or additional nonlinearity, such as arises from laser-cooling.

These calculations were carried out with a small, linear damping term that models the more complicated energy dissipation in real ion traps, but the main results should not be sensitive to the mechanism of dissipation, or to the value of the damping parameter, provided that it is small. The role of dissipation was examined in more detail for the manifold intersection at $q = 0.863$. The damping parameter can be varied over the range $\Gamma = 1 \times 10^{-4}$—$1 \times 10^{-3}$ and the intersection is always present at nearly the same location in phase space. Much the same behavior was found in previous studies of the stable, frequency-locked attractors of the Mathieu-Coulomb equations [23], in which the solutions for finite damping transformed smoothly as $\Gamma \to 0$ to solutions of the Hamiltonian equations of motion. This is reminiscent of the situation in celestial mechanics, in which extremely weak dissipation, acting over long periods of time, often results in trajectories being attracted to frequency-locked orbits [38] that are essentially identical to the solutions of Hamiltonian equations.

In locating the mediating orbits, we were guided by numerical simulations in which (as shown in Fig. 8) the mediating orbits are visible as a "skeleton" underlying the transition from chaotic to regular motion. The possibility exists to observe experimental trajectories in enough detail see these fine features of the motion, by using the Paul trap for microspheres. Because the Mathieu-Coulomb equations depend on the trapped particles' charge and mass only through the dimensionless combinations a and q, microspheres obey the same equations of motion as ions; they are subject to linear, aerodynamic drag, and also exhibit order-chaos transitions [27]. For dynamical studies, trapped microspheres and ions provide complementary information: the coarse features of the ions' motion can be observed over billions of trap cycles but the fine details of the trajectories are not seen, whereas the motion of microspheres can easily be resolved on the time scale of one trapping cycle. This capability has been exploited in the study of stable, periodic orbits that had eluded detection in ion traps [22] and it may provide more information about the unstable orbits underlying the boundary crisis.

APPENDIX: HEURISTIC DERIVATION OF EQ. (20)

We begin by sketching the argument of Ref. [11], relating the critical exponent to the eigenvalues of the monodromy matrix of $\mathbf{x}_A$ for a heteroclinic boundary crisis in a two-dimensional mapping, and then consider its application to our four-dimensional geometry. Referring to

Fig. 1, note that the lenticular area defined by the segments of $W^U(A)$ and $W^S(B)$ between the points $\mathbf{p}$ and $\mathbf{p}'$ encloses points that were once near the chaotic repeller but lie within the basin of attraction of the regular attractor. Approximating the arc of $W^U(A)$ that protrudes across $W^S(B)$ by a quadratic curve, it follows that if the height of the arc is r, then the distance between $\mathbf{p}$ and $\mathbf{p}'$ along $W^S(B)$ is proportional to $\sqrt{r}$ and the enclosed phase-space volume is $V \sim r^{3/2}$. The preiterates of this region under the mapping accumulate at $\mathbf{x}_A$ and the volume V_n of the nth preiterate is determined by the linear mapping at $\mathbf{x}_A$, provided that n is large enough. Since the segment $\mathbf{p}'$ lies along the expanding direction of $W^U(A)$ (with unstable eigenvalue λ_1) the corresponding dimension in the nth preiterate is $\sqrt{r}/|\lambda_1|^n$. Similarly, the height of the arc scales as $r/|\lambda_2|^n$, where λ_2 is the stable eigenvalue. The volume of the nth preiterate is thus

$$V_n \sim \frac{r^{3/2}}{|\lambda_1|^n|\lambda_2|^n}. \tag{A1}$$

This volume represents a region in the neighborhood of the chaotic repeller which escapes from the repeller after a short time (about n iterations of the map), i.e., it is proportional to the escape rate $T^{-1}(q)$ that appears in Eq. (13). When q is varied $W^U(A)$ and $W^S(B)$ change smoothly, and for small variations we can assume $r \sim (q_c - q)$. Consider the new volume V' obtained by the rescaling $r \to |\lambda_2|r$. Its $(n+1)$st preiterate, V'_{n+1}, has a volume

$$V'_{n+1} \sim \frac{r^{3/2}}{|\lambda_1|^{n+1}|\lambda_2|^{n-1/2}}, \tag{A2}$$

so the ratio of escape rates for $\alpha_2 r$ and r is

$$V'_{n+1}/V_n = \lambda_1^{-1}\lambda_2^{1/2}. \tag{A3}$$

From the scaling law, Eq. (14), this ratio is just $|\lambda_2|^\gamma$, which leads to the expression

$$\gamma = \frac{1}{2} - \ln(|\lambda_1|)/\ln|\lambda_2| \tag{A4}$$

for heteroclinic crises of two-dimensional maps.

Generalizing to a mapping in D dimensions, if $W^U(A)$ has dimension $D-1$ then it follows that $W^U(A)$ and $W^S(B)$ together bound a D-dimensional volume in phase space. Again this volume encloses a set of points that originate near the repeller but escape from it, and the critical exponent can be derived by considering how it scales with $q_c - q$, exactly as for $D = 2$ [12], yielding an equation similar to Eq. (A4). For our geometry, $W^U(A)$ is a two-dimensional hypersurface, and together with $W^S(B)$ it does not define the boundary of a four-dimensional volume in phase space, so we cannot apply directly the argument presented above. There still exists, however, a nonvanishing volume within the basin of attraction of the crystal containing points that were once in the neighborhood of the repeller, since otherwise the chaotic motion would not be transient. Assume that near $\mathbf{p}$ and $\mathbf{p}'$ these points surround $W^U(A)$ in a sheet of thickness s, where s does not depend on $q_c - q$. The four-dimensional volume that plays the role of V in the preceding paragraph is thus defined by segments of length $\sim r$ and $\sim s$ along the contracting direction of $W^U(A)$ and two segments $\sim \sqrt{r}$ along the expanding direction. Its nth preiterate has a volume

$$V_n \sim \frac{r}{|\lambda_U|^{2n}}\frac{rs}{|\lambda_S|^{2n}}. \tag{A5}$$

Again scaling $r \to |\lambda_S|r$ and taking the $(n+1)$st preiterate gives a new volume

$$V'_{n+1} \sim \frac{|\lambda_S|r}{|\lambda_U|^{2n+2}}\frac{|\lambda_S|rs}{|\lambda_S|^{2n+2}}. \tag{A6}$$

Identifying $V'_{n+1}/V_n = |\lambda_S|^\gamma$ as before yields Eq. (20).

[1] F. Diedrich, E. Peik, J. M. Chen, W. Quint, and H. Walther, Phys. Rev. Lett. **59**, 2931 (1987).

[2] D. J. Wineland, J. C. Bergquist, W. M. Itano, J. J. Bollinger, and C. H. Manney, Phys. Rev. Lett. **59**, 2935 (1987).

[3] J. Hoffnagle, R. G. DeVoe, L. Reyna, and R. G. Brewer, Phys. Rev. Lett. **61**, 255 (1988).

[4] R. Blümel, J. M. Chen, E. Peik, W. Quint, W. Schleich, Y. R. Shen, and H. Walther, Nature (London) **334**, 309 (1988).

[5] R. G. Brewer, J. Hoffnagle, R. G. DeVoe, L. Reyna, and W. Henshaw, Nature (London) **344**, 305 (1990).

[6] R. Blümel, C. Kappler, W. Quint, and H. Walther, Phys. Rev. A **40**, 808 (1989).

[7] R. G. Brewer, J. Hoffnagle, and R. G. DeVoe, Phys. Rev. Lett. **65**, 2619 (1990).

[8] T. Tél, in *Directions in Chaos,*, edited by Hao Bai-Lin (World Scientific, Singapore, 1990), Vol. 3.

[9] C. Grebogi, E. Ott, and J. A. Yorke, Phys. Rev. Lett. **48**, 1507 (1982).

[10] C. Grebogi, E. Ott, and J. A. Yorke, Physica **7D**, 181 (1983).

[11] C. Grebogi, E. Ott, and J. A. Yorke, Phys. Rev. Lett. **57**, 1284 (1986).

[12] C. Grebogi, E. Ott, F. Romeiras, and J. A. Yorke, Phys. Rev. A **36**, 5365 (1987).

[13] W. L. Ditto, S. Rauseo, R. Cawley, C. Grebogi, G.-H. Hsu, E. Kostelich, E. Ott, H. T. Savage, R. Segnan, M. L. Spano, and J. A. Yorke, Phys. Rev. Lett. **63**, 923 (1989).

[14] J. C. Sommerer, W. L. Ditto, C. Grebogi, E. Ott, and M. L. Spano, Phys. Lett. A **153**, 105 (1991).

[15] J. C. Sommerer, E. Ott, and C. Grebogi, Phys. Rev. A **43**, 1754 (1991).

[16] J. C. Sommerer and C. Grebogi, Int. J. Bifurc. Chaos Appl. Sci. Eng. **2**, 383 (1992).

[17] H. G. Dehmelt, Adv. At. Mol. Phys. **3**, 53 (1967); **5**, 109 (1969).

[18] G. Baumann, Phys. Lett. A **162**, 464 (1992).
[19] J. E. Howard and D. Farrelly, Phys. Lett. A **178**, 62 (1993).
[20] G. Baumann and T. F. Nonnenmacher, Phys. Rev. A **46**, 2682 (1992); D. Farrelly and J. E. Howard, *ibid.* **48**, 851 (1993); R. Blümel, *ibid.* **48**, 854 (1993); G. Baumann and T. F. Nonnenmacher, *ibid.* **48**, 856 (1993).
[21] R. Blümel, Phys. Lett. A **174**, 174 (1993).
[22] J. Hoffnagle and R. G. Brewer, Phys. Rev. Lett. **71**, 1828 (1993).
[23] J. Hoffnagle and R. G. Brewer, Science **265**, 213 (1994).
[24] A. W. Vogt, Phys. Rev. A **49**, 657 (1994).
[25] R. Casdorff and R. Blatt, Appl. Phys. B **45**, 175 (1988).
[26] J. D. Prestage, A. Williams, L. Maleki, M. J. Djomehri, and E. Harabetian, Phys. Rev. Lett. **66**, 2964 (1991).
[27] R. F. Wuerker, H. Shelton, and R. V. Langmuir, J. Appl. Phys. **30**, 342 (1959).
[28] E. Fischer, Z. Phys. **156**, 1 (1959).
[29] *Handbook of Mathematical Functions*, edited by M. Abramowitz and I. A. Stegun (U. S. GPO, Washington, D.C., 1968).
[30] J. W. Emmert, M. Moore, and R. Blümel, Phys. Rev. A **48**, 1757 (1993).
[31] A. W. Vogt, Appl. Phys. B **58**, 57 (1994).
[32] W. Neuhauser, M. Hohenstatt, P. Toschek, and H. Dehmelt, Phys. Rev. Lett. **41**, 233 (1978).
[33] S. Ichimaru, Rev. Mod. Phys. **54**, 1017 (1982).
[34] J. P. Gordon and A. Ashkin, Phys. Rev. A **21**, 1606 (1980).
[35] T. Sauter, H. Gilhaus, I. Siemers, R. Blatt, W. Neuhauser, and P. E. Toschek, Z. Phys. D **10**, 153 (1988).
[36] R. G. DeVoe, J. A. Hoffnagle, and R. G. Brewer, Phys. Rev. A **39**, 4362 (1989).
[37] J.-P. Eckmann and D. Ruelle, Rev. Mod. Phys. **57**, 617 (1985).
[38] J. Wisdom, Icarus **72**, 241 (1987).
[39] A. J. Lichtenberg and M. A. Lieberman, *Regular and Stochastic Motion* (Springer, New York, 1983).
[40] T. S. Parker and L. O. Chua, *Practical Numerical Algorithms for Chaotic Systems* (Springer, New York, 1989).
[41] N. H. Press, B. P. Flannery, S. A. Teukolsky, and W. T. Vetterling, *Numerical Recipes* (Cambridge University Press, Cambridge, 1987).

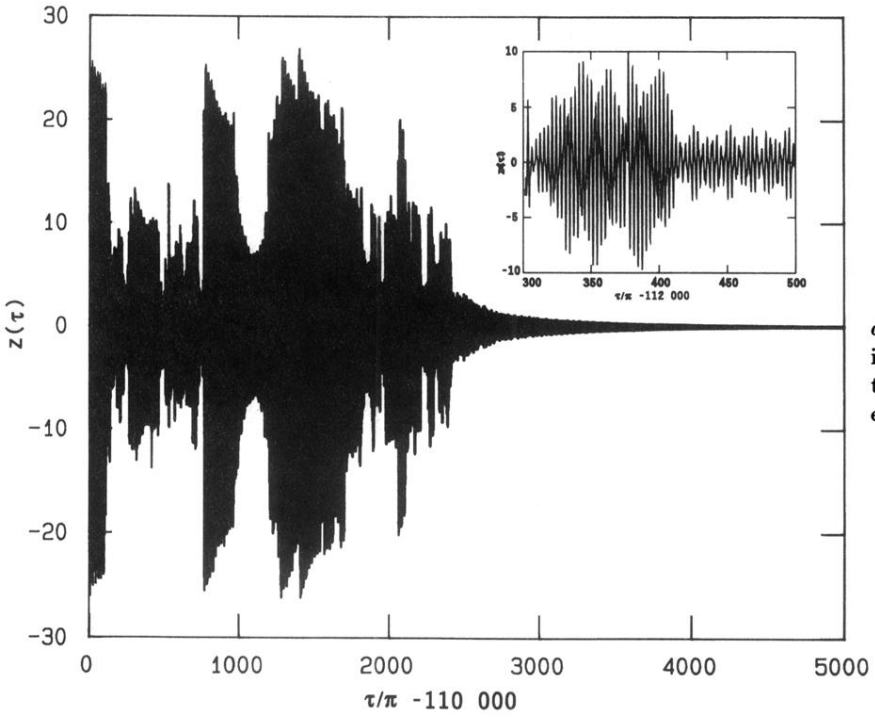

FIG. 6. Numerical solution of Eqs. (6) for $a = 0$, $q = 0.81$, and $\Gamma = 1 \times 10^{-3}$, showing the end of a chaotic transient with a lifetime of approximately $112\,400\pi$. The inset expands the last cycles of the transient.